Inorganic Chemistry

pubs.acs.org/IC

Article

Formation of Type II Silicon Clathrate with Lithium Guests through Thermal Diffusion

Yinan Liu, Joseph P. Briggs, Ahmad A. A. Majid, Thomas E. Furtak, Michael Walker, Meenakshi Singh, Carolyn A. Koh,* P. Craig Taylor, and Reuben T. Collins

Cite This: *Inorg. Chem.* 2023, 62, 6882−6892

Read Online

ACCESS | Metrics & More | Article Recommendations | Supporting Information

ABSTRACT: At low guest atom concentrations, Si clathrates can be viewed as semiconductors, with the guest atoms acting as dopants, potentially creating alternatives to diamond Si with exciting optoelectronic and spin properties. Studying Si clathrates with different guest atoms would not only provide insights into the electronic structure of the Si clathrates but also give insights into the unique properties that each guest can bring to the Si clathrate structure. However, the synthesis of Si clathrates with guests other than Na is challenging. In this study, we have developed an alternative approach, using thermal diffusion into type II Si clathrate with an extremely low Na concentration, to create Si clathrate with Li guests. Using time-of-flight secondary-ion mass spectroscopy, X-ray diffraction, and Raman scattering, thermal diffusion of Li into the nearly empty Si clathrate framework is detected and characterized as a function of the diffusion temperature and time. Interestingly, the Si clathrate exhibits reduced structural stability in the presence of Li, converting to polycrystalline or disordered phases for anneals at temperatures where the starting Na guest Si clathrate is quite stable. The Li atoms inserted into the Si clathrate lattice contribute free carriers, which can be detected in Raman scattering through their effect on the strength of Si−Si bonds in the framework. These carriers can also be observed in electron paramagnetic resonance (EPR). EPR shows, however, that Li guests are not simple analogues of Na guests. In particular, our results suggest that Li atoms, with their smaller size, tend to doubly occupy cages, forming "molecular-like" pairs with other Li or Na atoms. Results of this work provide a deeper insight into Li guest atoms in Si clathrate. These findings are also relevant to understanding how Li moves through and interacts with Si clathrate anodes in Li-ion batteries. Additionally, techniques presented in this work demonstrate a new method for filling the Si clathrate cages, enabling studies of a broad range of other guests in Si clathrates.

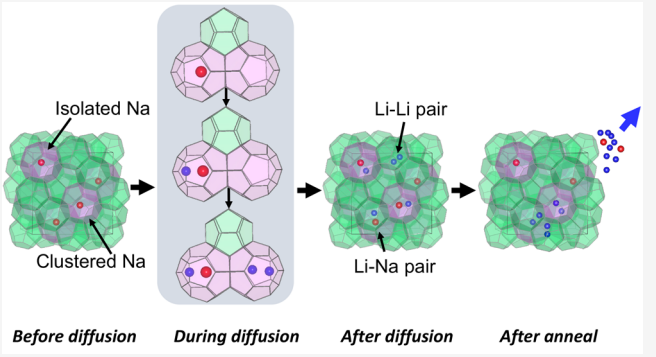

1. INTRODUCTION

Si clathrates are inclusion compounds with an open-cage Si-host framework that can trap guest atoms.[1] Room temperature and atmospheric pressure metastable Si clathrates are synthesized as either type I (M_8Si_{46}) or type II (M_xSi_{136}, $0 < x < 24$, M = guest atom species) phases.[1,2] If a clathrate can be synthesized with a sufficiently low guest atom concentration, it becomes a Si allotrope, an alternative to diamond Si (*d*-Si) with potentially important optical and electronic properties.[3−5]

Type II Si clathrate, for example, is predicted to be a semiconductor with a direct or nearly direct optical band gap near 2.0 eV,[6,7] and experimental results confirm both a larger band gap and a much larger absorption coefficient than those of *d*-Si.[3,8−11] Guest properties are also of interest. At low concentrations, the guests become shallow dopants to be used in device applications.[12] They may also have spin properties relevant to quantum information science.[12] To develop a fundamental understanding of the Si clathrates and associated guest properties and to ultimately harness their potential in applications require the ability to achieve low and tunable guest concentrations and to vary the guest species. Realizing low concentrations has, however, been problematic with many guests. While the synthesis of type I and II Si clathrates with a number of alkali metal (e.g., Na, K, Li, and Cs) and alkaline-earth metal (e.g., Ba and Sr) guests have been reported,[1,2,13−20] in general, the guest concentrations are too large to access the semiconducting properties of the Si framework, and the resulting materials are effectively metals.[21−23] The main exception to this has been type II Si clathrate with Na guests (Na_xSi_{136}), where Na can leave the structure after synthesis, and Na concentrations in the $10^{18}/cm^3$ range have been

Received: October 19, 2022
Published: January 30, 2023

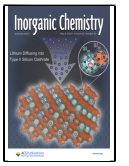

https://doi.org/10.1021/acs.inorgchem.2c03703
Inorg. Chem. 2023, 62, 6882−6892

reported.[12,24] This has moved type II Si clathrate into the regime of a heavily doped semiconductor and made it possible to study the electron binding energy[4] and spin characteristics of isolated Na atoms as dopants.[12]

In this study, we explore thermal diffusion into an extremely low-Na-content type II Na_xSi_{136} ($x \sim 0.009$) as a new approach to preparing Si clathrate with low concentrations of different guest atoms. We focus on Li as an alternative guest. The major barrier to the direct formation of Li-guest Si clathrates is that unlike Si−Na clathrates, which have been formed through thermal decomposition of a Zintl precursor NaSi phase,[25−27] the Si−Li phase diagram is more complex.[28,29] An equivalent Li silicide phase, which can decompose into type II Li_xSi_{136} clathrate, has not been demonstrated yet. With diffusion, the situation is different. Type II Si clathrates consist of face-sharing Si_{20} and Si_{28} polyhedra.[30] The unusual cagelike Si clathrate structure creates naturally occurring paths that can facilitate atomic or ionic transport into and out of the material without large changes in volume and associated defect formation.[30,31] In addition, the amount of guest atoms introduced in the material by diffusion is controllable, with K_xGe_{136} (x = 8.6 or 24) obtained previously by diffusing K vapor into the almost empty Ge_{136} structure.[32] Using time-of-flight secondary-ion mass spectroscopy (TOF-SIMS), we confirm Li diffusion into the Si clathrate film and estimate the effective diffusion constant of Li across the film. Using Raman scattering spectroscopy and X-ray diffraction (XRD), we investigate the interaction of Li with the Si framework and the stability of the Si−Li system. Our electron paramagnetic resonance (EPR) results on Li-doped Si clathrate films suggest that the Li guests behave differently from Na in the cages. We find evidence that Li tends to pair with Na and other Li atoms in the lattice, suggesting multiple occupancy and cluster formation with associated inhomogeneity at an early stage of Li insertion.

The focus of this work is on the initial stage of Li diffusion, when the clathrate cages are intact, and studying how Li interacts with the structure. Results of this work, however, provide insights into the effects of Li guest atoms on the Si clathrate lattice for potential electrochemical applications. For example, ion motion is critical to battery anode operation, with *d*-Si and amorphous Si (*a*-Si) showing limitations associated with the significant volume expansion of nearly 300% after lithiation, causing instability or even pulverization of the Si anodes.[33] Si clathrates have been proposed and studied as potentially promising anode materials,[31,34,35] and theoretical calculations suggest that the lattice constant of type II Si clathrate should increase very slightly after electrochemical Li insertion.[36] However, issues like those in *d*-Si have been reported, with amorphous phases forming after repeated cycling of Li into and out of Si clathrate anodes.[34,37−39] This amorphous phase transformation prevents the reliable use of Si clathrates as anodes and complicates the characterization of Si−Li clathrates. Elucidation of the amorphous phase transformation due to Li diffusing into and out of the cages relies on a fundamental study of the interaction of Li with the clathrate structure. This study sets the stage for a more detailed understanding of Li ionic diffusion in the Si clathrate lattice. Techniques here also demonstrate a novel method for filling the Si clathrate cages and allowing more potentially interesting guests to be studied.

2. EXPERIMENTAL METHOD

The Li-doped Si clathrate samples were prepared through thermal diffusion of Li into Si clathrate films with extremely low Na content. The synthesis of Na guest type II Si clathrate films follows a two-step method that is adapted from powder synthesis.[40] Here we briefly summarize the approach that is described in detail in ref 9. Films were formed on ⟨100⟩, n-type Czochralski Si wafers doped with phosphorus (5−10 Ω·cm) or arsenic (15 Ω.cm). All of the procedures below were conducted in an Ar-purged glovebox or in a tube furnace (with flowing Ar or under vacuum). The first step is forming NaSi film on the Si substrate in a Ta crucible (99.95% purity), as shown in Figure S1. A preliminary annealing step (600 °C for 30 min under flowing Ar) on the empty Ta crucible was used with the goal of removing the O and moisture trapped in the metal. Subsequently, a layer of Na (99% purity, Na cubes, Sigma-Aldrich) was placed on the bottom of the crucible. After that, a 12 × 25 mm^2 wafer was washed using methanol, acetone, and deionized (DI) water and then horizontally placed on the stage of the Ta crucible that is about 5 mm above the Na layer. The crucible was then covered by the Ta lid and sealed by wrapping the crucible in 99% pure Al foil, which helps to prevent Na vapor from leaving. The sealed crucible was then placed in a quartz furnace tube and heated at 550 °C for 1 h under flowing ultrahigh-purity Ar to form a NaSi layer on the surface of the substrate. During the second step, the resulting Si wafer, with NaSi film on the surface, was heated at 400 °C under vacuum (10^{-6} Torr) in a quartz furnace tube for 24 h to decompose into the Si clathrate phase, followed by a 48 h anneal at 450−470 °C to further remove the excess Na.

As-prepared Si clathrate films contained some disordered Si phase,[9,41] especially on the top surface, which appears to be about 2−3 μm thick under a scanning electron microscope.[9] Therefore, the films were rinsed with ethanol and DI water, followed by a 2 min SF_6 dry etch in a reactive ion etcher at a pressure of 0.4 Torr and a microwave power of 250 W at 13.56 MHz.[9] The SF_6 etch removes the surface layer and further reduces the Na concentration.[9] After etching, the film thickness is about 6−8 μm. The XRD pattern of the film after etching and its Rietveld refinement analysis are given in Figure S2. The estimated Na content corresponds to $x \sim 0.96$. However, because XRD loses its sensitivity to the Na content as x approaches 1,[5] we do not consider this value to be accurate. Instead, EPR was used, as discussed in ref 12, to more accurately determine the Na level through a spin density calculation, which gives a total Na concentration of about 3 × 10^{18}/cm^3 ($x \sim 0.009$ in Na_xSi_{136}). This pushes the Si clathrate into a regime where it can be regarded as a heavily doped semiconductor.[12] More importantly, for the present study, this indicates that the large and small cages of the Si clathrate are essentially guest-free.

Li-diffused Si clathrate films were prepared following methods similar to those used for diffusing Li into *d*-Si.[42] A 6 × 25 mm^2 bare Si wafer was coated with a roughly 50-μm-thick layer of Li metal (99.9% purity, Li ribbon, Sigma-Aldrich). A Si clathrate film that had the same size as the wafer was used to cover the Li layer with the Si clathrate film in contact with the Li metal, forming a sandwich (Si clathrate film/Li layer/Si wafer), as shown in Figure S3. This was followed by wrapping the sandwich layers together using Ta foil (0.0127 mm thick, 99.95% purity). The sandwich was then inserted into a quartz tube (10 mm inner diameter). A vacuum valve mounted on an O-ring-sealed quick connect was then coupled to the open end of the tube. All of the procedures above were performed in an Ar-purged glovebox. The quartz tube was valved off before removal from the glovebox to avoid exposure to air. The quartz tube with the sandwiched sample inside was then flame-sealed under vacuum (10^{-6} Torr). Subsequently, the sealed ampoule was annealed at 250−400 °C in the tube furnace. The annealing time varied from 2 to 24 h for different samples. The ampoule was quenched in water immediately after annealing to minimize Li motion as the sample cooled down. The ampoule was then returned to the glovebox. The sample was removed from the ampoule and brought out into air. At this point, there was reactive material on the surface. This was removed by

https://doi.org/10.1021/acs.inorgchem.2c03703
Inorg. Chem. 2023, 62, 6882−6892

initially atomizing DI water drops onto the surface, followed by rinsing the whole film in DI water until no bubbles formed. In an alternative annealing method, the wrapped sandwich structure was inserted into a 1-in. quartz furnace tube while in the glovebox. The tube was sealed with end-caps, removed from the glovebox, installed in the tube furnace, and evacuated under dynamic vacuum during sample heating. For convenience, the sample before diffusion is called "Na-doped", while the sample after diffusion is called "Li-doped".

The samples were characterized using XRD, Raman scattering spectroscopy, and TOF-SIMS. The use of these and other structural characterization techniques is outlined in ref 9. An X-band Bruker EMX EPR instrument was used to detect the low-concentration guests and change of the defect state in the samples. The EPR system was equipped with a Bruker ColdEdge closed-cycle He cryostat. In this work, measurements were performed from 5 to 300 K.

3. RESULTS AND DISCUSSION

3.1. Effective Diffusion Constant. We used TOF-SIMS to detect the ion profiles across the film. Parts a and b of Figure 1 present the normalized intensities of detected secondary ions

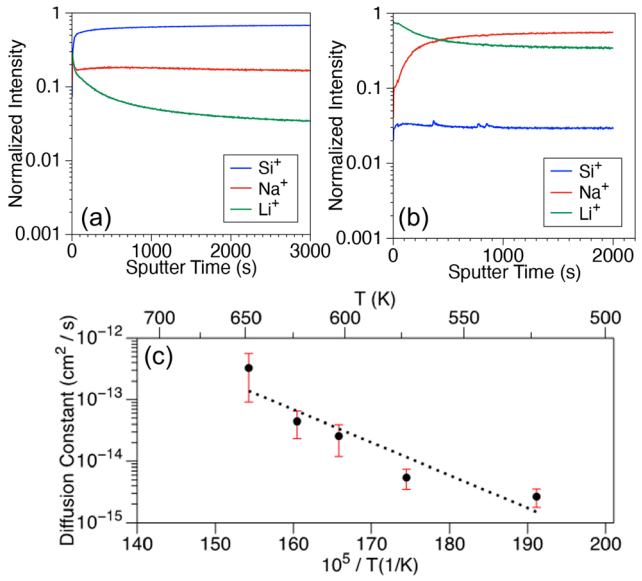

Figure 1. (a and b) Normalized intensities of detected secondary ions for the Li films that were diffused at 375 °C for 2 h and at 360 °C for 5 h, respectively. The weak peaks in part c are due to an artifact. The measurements were all performed with a primary ion (Bi^+) energy of 30 keV and a sputtering ion (O_2^+) energy of 0.5 keV. (c) Effective diffusion constant of Li in the Si clathrate film versus the reciprocal of absolute temperature. The dashed line is an exponential fit of the diffusion constant. The fitting equation is $D_{Li} = 2.3887 \times 10^{-5} e^{-12288/T}$, where D_{Li} is the diffusion constant (cm^2/s) and T is the absolute temperature (K).

of Li, Na, and Si from samples that were diffused at 375 °C for 2 h and 360 °C for 5 h, respectively. In each case, the sputtering area was a 150 × 150 μm^2 region. The profiles clearly show that Li is present in the films after diffusion. Different from Na guests, the Li intensity drops from the top surface, showing a diffusion-like profile. In a comparison of the Li profiles of Figure 1a,b, the intensity in Figure 1b is more uniform beyond the surface than that in Figure 1a, consistent with the longer diffusion time (5 h) for the sample in Figure 1b. The drop in the Na intensity near the surface in Figure 1b is due to some Na atoms leaving the film during the long-time diffusion, which is observed in multiple samples and supported by the EPR results after long-time anneals as discussed later.

We were able to form Li-diffused Si clathrate samples with different Li contents. The Li intensity could be more than 10 times less than the Na intensity or stronger than the Na intensity in TOF-SIMS profiles of different samples. In interpreting the ion yields, however, it is important to note that the yield is affected by the electron affinity, ionization potential, and atomic mass as well as the sputtering parameters[43−45] and hence varies from element to element. Because we do not yet have standards to allow us to calibrate the elemental yields for various ions in type II Si clathrate films and yields can be further affected by the sample roughness and voids present in these kinds of films, the relative intensities of Si, Li, and Na in the films are not representative of the actual relative elemental concentrations in the film, although we expect Li and Na to be moderately close because they have quite close ion yields in crystalline Si (*c*-Si).[43] The typical Na concentration in our films is about ~$10^{18}/cm^3$, and this gives an idea of the range of Li contents after diffusion. We also expect the yields of both Li and Na to be higher than that for Si. The profile of a given element across the film, however, is representative of its concentration profile and can be used to estimate a diffusion coefficient.

SIMS also shows quite a bit of inhomogeneity in the ion intensity from one spot to another. In prior work, we associated regions of high Na content with cracks and grain boundaries in the undiffused films.[9] These interfacial regions are also found to be more defective.[9] For diffusion temperatures above 350 °C, regions of high Na and Li levels appear to be correlated (Figure S4). The profiles in Figure 1b come from one of those areas with relatively high Na and Li contents, resulting in higher ion intensities of Li and Na relative to Si. We have fit the SIMS profiles from the samples that were diffused for 2 h at different temperatures to extract effective diffusion constants in Figure 1c, as discussed next. However, because of the issues discussed above, the values obtained may not be intrinsic to the clathrate material but rather representative of both the diffusion coefficient and morphological properties of the films. Nevertheless, the values place a bound on the diffusion coefficients and are useful for predicting how temperature and time effect thermal incorporation of Li in this kind of film.

To estimate the effective Li diffusion constant, we used the one-dimensional solution of the diffusion equation assuming that the Li concentration at the surface is constant throughout the diffusion, $N(x, t) = N_0 \operatorname{erfc}\left(\frac{x}{2\sqrt{D_{Li}t}}\right)$, where N_0 is the Li intensity at the film surface, D_{Li} is the diffusion constant of Li that depends on the annealing temperature, and $N(x,t)$ is the Li concentration after annealing for a time t at a distance x from the surface. To calibrate the sputtering depth, we did a long scan (~35000 s) using the same parameters and measured the depth of the etch pit using a profilometer, which was about 5 μm (±0.6 μm). We then calibrated the sputtering depth of other TOF-SIMS profiles obtained with the same parameters. This depth calibration showed that the SIMS measurements are always in the clathrate film, not reaching the Si substrate, although we believe that Li diffuses all the way through the clathrate film. The reason is that we used carbon tape to lift most of the film off the substrate and performed TOF-SIMS on the buried surface, which was originally close to the interface between the film and the *d*-Si

https://doi.org/10.1021/acs.inorgchem.2c03703
Inorg. Chem. 2023, 62, 6882−6892

substrate. We still saw the presence of Li even though its intensity was very low.

The results of the effective diffusion constants are presented as an Arrhenius plot in Figure 1c. These values used ion yields from the full 150 × 150 μm^2 sampling region. Error bars were estimated in two ways. For the first, two samples were diffused at the same temperature (375 °C) for the same length of time. For the second, we roughly divided the sampling area, laterally, into smaller 50 × 50 μm^2 regions of interest and fit the profiles in each of these smaller regions. As noted above, the samples exhibit an inhomogeneous Li concentration. It was found that subregions with higher Li content had a systematically higher diffusion coefficient than subregions with lower Li content. We speculate that the regions with higher Li content are near grain boundaries and cracks and are more defective. This would suggest that values from low-Li-content regions might be closer to intrinsic. The errors estimated by both methods were comparable; hence, the error bars in Figure 1c were created using the high- and low-Li-content values from regions of interest. Within this error and for the temperature range explored, the diffusion constant exhibited Arrhenius behavior. We note that the measured effective diffusion constants obtained for Li in Si clathrate were less than those previously reported for *d*-Si[42,46] in the temperature range that we studied.

3.2. Raman Scattering Study of Li-Doped Si Clathrate. A type II Si clathrate structure is made up of Si_{20} small cages and Si_{28} large cages. For the low Na concentrations in this work, prior studies found that Na guests are only present in the large cages.[22,40] Previous theoretical calculations indicate that inserted Li can reside in both large and small cages, although it is energetically favorable for Li to occupy the small cages over the large cages.[36] Isolated Li atoms in both the large and small cages should contribute rattle modes to the phonon density of states, although only those in the large cages would be Raman-active.[14] Technically Raman spectroscopy should allow direct detection of Li guests if they are present in large cages in sufficient concentration. Rattle modes, however, occur at low frequency and have been difficult to detect in Raman spectroscopy. The presence of Li can, instead, be detected indirectly through its effect on the Si cage modes. This is illustrated in Figure 2. The top spectrum obtained from the starting Na_xSi_{136} before Li diffusion is in very good agreement with published results where the symmetries of the modes have been identified in conjunction with model calculations.[13,14,47] The three spectra at the bottom of the figure were typical of those obtained from the surface after Li diffusion. Spot 1 is essentially the normal Si clathrate spectrum with a slight red shift in all of the modes (blue curve), and regions like spot 2 were also commonly observed, showing a Si clathrate spectrum shifted much more significantly to lower frequency (green curve). We attribute these red shifts to the presence of Li. Spot 3 shows a spectrum that we have previously identified as arising from disordered or "amorphous-like" Si (red curve).[9] Disordered spectra arose from areas that appeared shiny under a Raman microscope. In the next section on stability, we return to the Raman measurements and the increase in the amount of disordered Si after Li diffusion, as supported by the increase of the shiny region in Raman spectroscopy. For the present discussion, we focus on those regions showing type II Si clathrate spectra, and the red shift in the Raman peaks.

To show that the softening of the vibrational frequencies is caused by Li diffusing into the Si clathrate structure, we annealed a film with Li dots (about 1 mm diameter, 0.5 mm thickness, and more than 8 mm between dots) in contact with the film surface instead of a continuous Li layer and acquired Raman spectra of the diffused film at different locations: spots in contact with the Li dots, regions near but not in contact with the Li, and regions far from the Li. As shown in Figure 3a, the film region in contact with the Li during annealing is converted to *d*-Si. This conversion to *d*-Si will be discussed in section 3.3. The film region around the Li dots (about 0.5 mm away from the dots) reproducibly exhibits a frequency reduction, as shown in the blue curve in Figure 3a. On the basis of estimates from the diffusion coefficients in Figure 1, lateral diffusion of Li through the film would be too small to dope the neighboring regions. Instead, it is likely that Li vapor transported laterally from the dots and diffused into the sample. Spectra from film regions far from the Li dots (about 3−5 mm away) showed the type II Si clathrate Raman spectrum of Na_xSi_{136}, like the spectrum prior to Li diffusion.

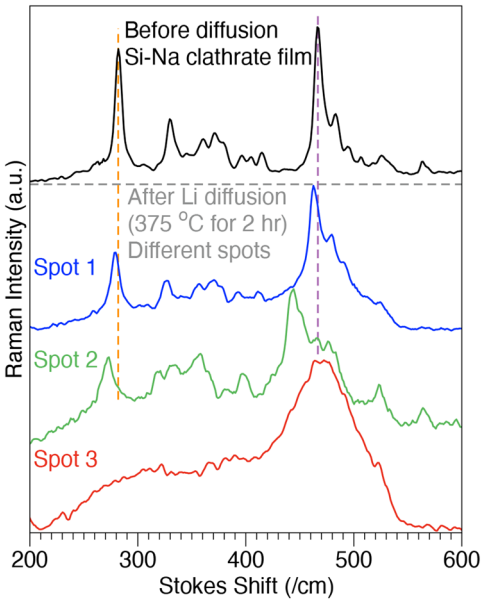

Figure 2. Raman scattering spectra of the Si clathrate film before (black curve) and after (blue, green, and red curves) Li diffusion. Three representative Raman spectra at different spots of the film after diffusion are presented. The orange and purple dashed lines at 282 and 466 cm^{-1} indicate the shift of the spectra after diffusion.

From these observations, we conclude that mode softening is associated with the presence of Li. A similar softening of vibrational modes with increasing guest concentration has been observed in neutron scattering studies[48] and Raman spectra of a Na guest Si clathrate[49] and in a type II Si clathrate prepared with Cs guests in the large cages.[14] In fact, this is not unique in type II Si clathrates. Raman lines in K-guest type I Si clathrates are noticeably down-shifted relative to their spectral counterparts in Na-guest materials. The former also has a higher guest occupancy.[50]

In these earlier studies and the Li-guest spectra presented here, higher-frequency vibrational modes, >350 cm^{-1}, show the largest decreases in frequency when the guest concentration increases. Nolas et al. have noted that these modes result from bond stretches of paired Si atoms on the cage.[14] They argued that, because the guests are donors, adding guests adds electrons to the antibonding conduction band states, causing a reduction of these vibrational frequencies.

https://doi.org/10.1021/acs.inorgchem.2c03703
Inorg. Chem. 2023, 62, 6882−6892

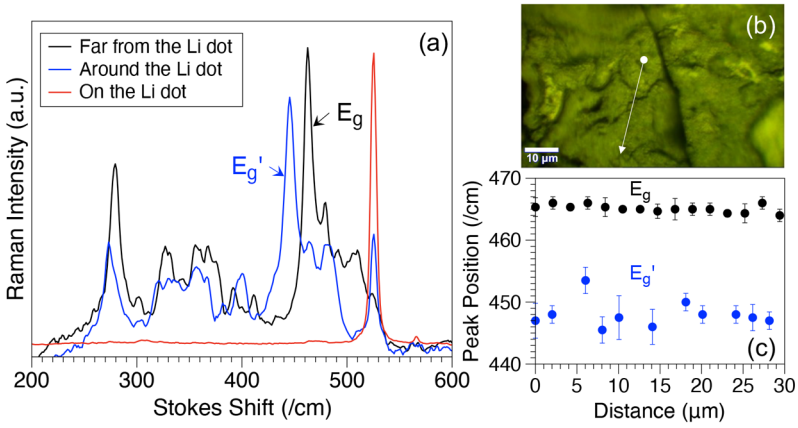

Figure 3. (a) Raman scattering spectra of different spots on a Si clathrate film that was annealed with Li dots at 375 °C for 3.5 h in a 1-in. quartz tube. The spectra were taken with 1.5 mW incident laser power and 400 s acquisition. The arrows point to the E_g symmetry peak in a type II Si clathrate and its counterpart E_g' after the shift. Four Li dots are placed on a piece of Si wafer. A Si clathrate film with the same size as the wafer was placed on top of the wafer to make a sandwich with the Si clathrate film in contact with the Li pieces. The sandwich was then placed in a 1-in. quartz tube and annealed in a tube furnace under dynamic vacuum. (b) Image of the Raman line scan trace on a grain near a Li dot (after diffusion). (c) Raman frequencies of the identified E_g symmetry peak along a line of a grain far from the Li dots (black) and E_g' along the scan line shown in part b (blue). Both scans are taken after diffusion. A total of 15 spectra at evenly spaced points along each scan line were taken, and each spectrum was acquired over 400 s. The error bars were obtained from three repeated line scans along the same line. The *x* axis is the distance from the starting point of the line scan. The missing points in the blue line scan of part c correspond to locations showing a strong *a*-Si feature that obscured the E_g mode location.

Returning to Figure 3a, it appears that a softening of the vibrational modes indicates not only the presence of Li guests but also the amount of Li that is present through the size of the shift. This suggests that Raman spectroscopy could be used to look for variations in the guest concentrations on length scales much smaller than, for example, those of the TOF-SIMS results presented above. This was investigated through line scans of Raman spectra on sample regions located far from the Li dots and in regions adjacent to the dots. Figure 3b shows an optical image of the scanned region near a Li dot. The lengths of the line traces were both around 30 μm. Spectra at 15 points evenly spaced along each line were acquired. Focusing on the dominant E_g mode indicated in Figure 3a, the frequency of the peak was plotted in Figure 3c as a function of the position along the scan line. As noted above, after diffusion, there was more disordered Si on the sample surface, and in a few instances, the disordered spectrum obscured the position of the E_g mode, so these points were not included. In Figure 3c, the black dots representing the peak positions far from the Li are closely clustered at about 465 cm^{-1}, while the blue dots representing the Li-diffused region show peak positions of 444−453 cm^{-1}, which are much more scattered. A similar Raman line-scan study of a type II Si clathrate sample before and after Li diffusion using our standard preparation with a continuous film of Li showed similar results (Figure S5). Taken together, these results indicate quite a bit of variation in the Li content of diffused samples on a micron length scale.

3.3. Stability of the Si−Li System. One of the most significant questions regarding Li insertion into Si clathrates concerns how Li affects the metastability of the Si clathrate structure. Previous work on electrochemical lithiation suggested that Si cages can be destroyed, forming disordered Si phases and crystalline Li silicide compounds after a few intercalation cycles.[37,38] Presumably this was due to the large amount of Li inserted and the effect of Li atoms moving into and out of the cages. Herein we study the stability of the Si−Li system during thermal diffusion at various temperatures (250−400 °C) and annealing times, which can affect the amount of Li inserted and the driving force for the phase transformation.

Conversion of the type II Si clathrate phase to *d*-Si usually occurs above 500 °C for low-Na-content material.[51,52] As part of the film synthesis process for this study, the starting Si clathrate films were annealed for 48 h at 450−470 °C in vacuum to remove excess Na. There was no evidence of *d*-Si formation after these anneals. We find, however, that the Li-diffused Si clathrate can convert to disordered or polycrystalline Si phases when annealed at much lower temperatures. This is illustrated using XRD in Figure 4. For this study, sample diffusions were performed as described above with a sandwich structure of clathrate film/Li/Si wafer. The Si−Li system was very stable for diffusion temperatures of 330 °C or less (Figure 4e) with no other phases observed by XRD. Comparing Figure 4d with Figure 4c, a 3.5 h diffusion at 350 °C gave no other obvious phases, while a 5 h Li diffusion process at the same temperature (Figure 4c) resulted in the emergence of the polycrystalline *d*-Si 111 peak near $2\theta = 28.5°$. At 375 °C, a 3.5 h Li diffusion converted some Si clathrate structure into polycrystalline *d*-Si (Figure 4b), and a 24 h diffusion fully transformed the cage structure into a polycrystalline *d*-Si phase (Figure 4a). We also performed Li diffusion at 400 °C and obtained only a polycrystalline phase after a 3.5 h short anneal (Figure S6). As a control, the XRD pattern in Figure 4f came from a film prepared in exactly the same way except the Li layer was not included. It was annealed at 375 °C for 24 h, and the resulting film was still high-quality type II Si clathrate with low Na content. These results suggest that decomposition into *d*-Si is an activated process in the Li-doped sample, with a higher rate (requiring less time) at higher temperatures, and that the activation barrier is reduced by the presence of Li. On the other hand, the formation of *d*-Si driven by Li diffusion is reminiscent of metal-induced crystallization[53] in which metal contamination can catalyze crystallization of Si at lower temperatures. Further investigations of Li-induced Si crystal-

https://doi.org/10.1021/acs.inorgchem.2c03703
Inorg. Chem. 2023, 62, 6882−6892

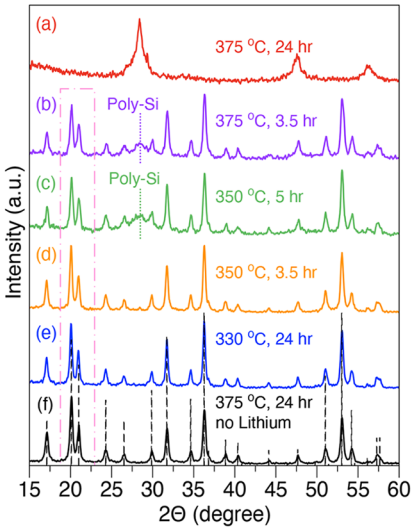

Figure 4. XRD patterns of Li-diffused films that were diffused at different conditions: 375 °C for 24 h (a), 375 °C for 3.5 h (b), 350 °C for 5 h (c), 350 °C for 3.5 h (d), 330 °C for 24 h (e), and 375 °C for 24 h without Li (f). The black dashed line represents the reference peaks of type II Si clathrate (ICDD 98-024-8181). The dotted lines indicate the presence of polycrystalline Si (Poly-Si). The pink dash-dotted box indicates the two peaks that are sensitive to the amount of alkali atoms (both Li and Na) in the material. The film was fully converted into polycrystalline Si in part a.

lization would be insightful for controlling the lithiation of Si clathrates both thermally and electrochemically.

Other interesting insights can be found in the XRD patterns in Figure 4. The XRD peak positions of Si clathrate did not change as a result of Li insertion. This is consistent with the simulated powder XRD patterns[36] of lithiated Si clathrate using different Li sites in the Si cages from Na atomic sites. Similarly, after diffusing K into low-Na-content Ge_{136} powders, the material exhibited the same peak positions in the XRD patterns as before.[32] Also of interest is the reduction in the intensities of the two peaks around $2\theta = 20°$ (in the pink dash-dotted box of Figure 4) relative to the rest of the peaks when Li is inserted in the film. For Na_xSi_{136} clathrate, the relative intensities of these two peaks are inversely correlated with the Na content when $x \geq 1$.[5,40] The XRD peak intensities of Na_xSi_{136} were computed by Sim using the structure factor of a type II Si−Na clathrate, which depends on the structure factor of Si and Na atoms as well as the Na concentration and distribution in the cages.[54] This makes a Rietveld refinement of XRD patterns from Na_xSi_{136} possible and allows x to be estimated. The structure factors of Li in the Si clathrate cages are different from those of Na due to distinct guest atomic positions, and there is no corresponding Li_xSi_{136} crystallographic data to help with an accurate refinement. It seems likely, however, that Li and Na are sufficiently similar to apply the same kind of model and that the decrease in the intensity of the two peaks around $2\theta = 20°$, relative to the rest of the pattern, is also indicative of a higher doping level in the Si clathrate structure caused by Li diffusion. We note that, in electrochemical studies of Li insertion, similar assumptions about the applicability of the Na_xSi_{136} model to Li guest material have been made.[36] A Rietveld refinement analysis of the XRD pattern of a Li-diffused sample was performed using Na_xSi_{136} and *c*-Si as standard phases, as shown in Figure S7. The results correspond to $x \sim 2.94$. Although the details of the fitting are suspect without an accurate Li-guest standard, the results are consistent with the presence of Li and an increase of doping after diffusion.

Raman spectroscopy provides additional evidence for increased Si clathrate instability during Li diffusion. As shown in the Raman spectra of Figure 3, most of the surface region exhibited a type II Si clathrate phase (black curve) before diffusion. After diffusion at 375 °C for 3.5 h, those regions in direct contact with the Li metal dots exhibited the Raman spectrum of *d*-Si. This is consistent with the XRD results in Figure 4, where polycrystalline *d*-Si features began to appear for the same temperature and annealing time. It also suggests that the polycrystalline Si initially formed at the surface in contact with the Li because the Raman spectra, which are more surface-sensitive, only showed *d*-Si, while XRD for the same conditions showed both clathrate and *d*-Si signatures.

In the region near, but not directly in contact with, the Li dots, inhomogeneity increased. In addition to type II Si clathrate spectra with a range of red shifts (discussed above), there was a significant increase in the prevalence of spectra attributable to disordered Si. This was true in the samples prepared both with Li dots and from a continuous layer of Li metal (Figure S5). Often the shifted Si clathrate spectra were superimposed on a disordered Si background, like the green curve in Figure 2, which was observed on multiple spots of different samples. We also exfoliated the top film surface as discussed in ref 9 to allow Raman spectra to be collected from the interior of the film. We found that the disordered Si regions only exist on the sample surface. In the XRD analysis above, we discussed the fact that both the temperature and annealing time effected how much of the Si clathrate decomposed during Li diffusion. The results of this Raman study indicate that the amount of Li introduced into the structure also plays a major role in the instability of the clathrate phase. For example, if we remove the Li source and anneal the Li-diffused samples, we can again anneal at temperatures as high as 450 °C without conversion to *d*-Si, as shown in the next section.

In addition to the thermally driven Li insertion in this work, previous electrochemical lithiation of clathrate reported similar structural changes.[34,37−39] An interesting observation in the electrochemical studies is that nearby Li−Si alloy phases like Li silicides or amorphous alloys can play a role in decomposition of the Si clathrate structure[31,37] Chan et al. reported, however, that Li−Si alloy formation does not occur before the insertion of 32 Li atoms per unit cell.[36] Results of the work suggest that, by controlling the Li amount inserted, the clathrate structure could be maintained with Li guests in the cages. Assuming that the same threshold applies for higher-temperature Li diffusion in this work, SIMS suggests that most of our film is below this Li level, so we should not expect too much alloy formation. The only place where the level might rise high enough is near the surface, and this is where we tend to see disordered material begin to form in Raman spectroscopy. After the thermal Li diffusion process, the air exposure and rinsing treatment we applied would remove the reactive silicide phases, so we would not expect to see the evidence of such phases in the XRD patterns presented in Figure 4. We also did XRD on Li-diffused films in a sealed sample holder, which prevents atmospheric exposure of the sample, but still did not see any peaks from Li−Si silicides or alloys. Therefore, we believe the Li−Si alloys/compounds are not the majority phase

https://doi.org/10.1021/acs.inorgchem.2c03703
Inorg. Chem. 2023, 62, 6882−6892

and may only exist near the film surface where the Li concentration is the highest compared with the material underneath. It is intriguing to speculate that the increase in disordered Si at the surface observed in Raman spectroscopy could be a weak remnant of a disordered Li−Si alloy. With a low enough Li content in the disordered phase to reduce reactivity, it is not removed by air exposure and post-synthesis rinsing steps.

3.4. EPR Study of Li-Doped Si Clathrate. An EPR spectrum of a low-Na-content (total spin density 3×10^{18}/cm^3) Si clathrate film (before Li diffusion) taken at 6 K is shown as the black curve of Figure 5. As previously discussed,[9,12] it has four strong hyperfine (HF) lines. They arise from the interaction of the electrons localized on the ^{23}Na atoms in the cages with the spin $^3/_2$ nuclear magnetic moment of ^{23}Na. Three additional weak lines are present near 318, 331, and 344 mT, which have been attributed to Na dimers even though the middle one is on top of a broad peak. There are actually seven lines from the two Na nuclei, with four of them hidden by the isolated ^{23}Na HF lines.[12] The broad peak near the center of the spectrum has been assigned to superimposed signals of clustered ^{23}Na.[5,12] This broad peak is actually the dominant feature in the spectrum, as is evident in the inset of Figure 5, where the curve is integrated to obtain an absorption spectrum. A defect line due to Si dangling bonds is centered at $g \sim 2.005$. Compared with previously reported EPR spectra of Si clathrates,[4,5,12,40,55] the ratio of the intensity of this *a*-Si defect line to the Na HF lines is much lower, with calculated *a*-Si spin density of 4×10^{16}/cm^3. This spectrum represents the starting material for our diffusion study.

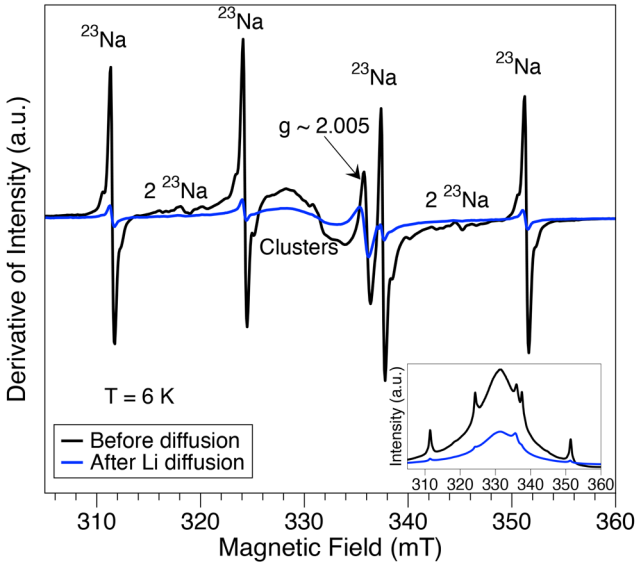

Figure 5. EPR spectra of Si clathrate films before and after Li diffusion. The film was annealed in the sealed quartz ampoule at 375 °C for 3.5 h during diffusion. Both spectra were taken at 6 K and averaged over five scans, with 10^4 gain and 20 dB attenuation. The two spectra were plotted at the same scale. The inset shows the integral of the two spectra over the entire field.

Li is in the same column as Na, so, like Na, is expected to donate a single electron to the Si framework. Also, the dominant Li isotope, ^{7}Li, has the same nuclear $^3/_2$ spin as ^{23}Na. After diffusion, if we assume that Li guests occupy cages in exactly the same way as Na guests, we might expect to observe a similar EPR spectrum, but with the HF coupling constant scaled by the ratio of the atomic HF coupling splitting of Li atoms to Na atoms. This is illustrated in Figure S8, which shows an EASYSPIN[56]-simulated EPR spectrum of isolated ^{7}Li atoms based on the assumptions above.

Surprisingly, in multiple diffusions, we see no direct signature of Li-related EPR lines. We can only see the evidence of Li indirectly through its effect on Na-related EPR features. This is evident in the blue curve in Figure 5, which is an EPR spectrum obtained after Li diffusion. The two spectra in Figure 5 were taken with the same parameters and plotted on the same scale. Li diffusion significantly suppressed the intensity of the Na HF lines. The broad peak due to clustered Na (inset in Figure 5) was also suppressed but not by as much as the isolated Na HF lines. The total spin density after Li

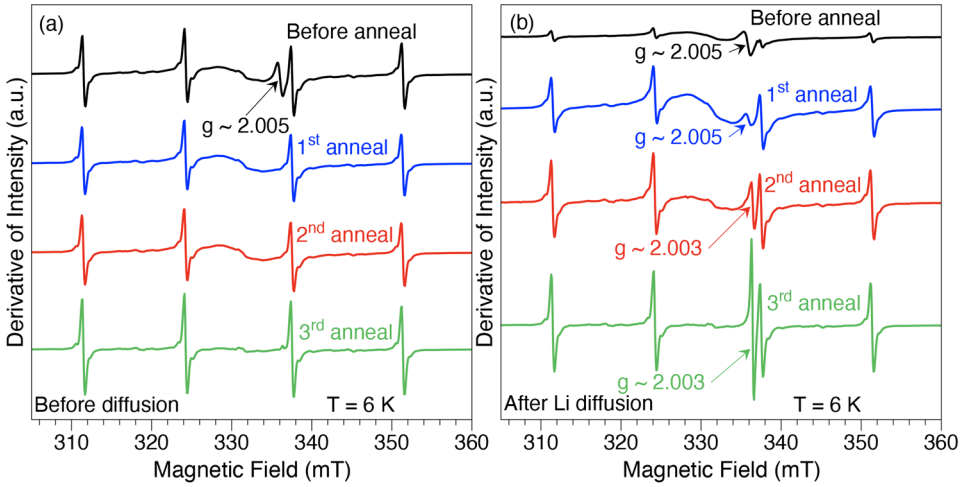

Figure 6. (a) EPR spectra of the Si−Na clathrate film (before diffusion) before and after a series of anneals in the sealed EPR tube. (b) EPR spectra of the Li-diffused clathrate film (375 °C for 3.5 h in the sealed ampoule) before and after a series of anneals in the sealed EPR tube. All of the spectra were taken at 6 K and averaged over five scans, with 10^4 gain and 20 dB attenuation. The samples were kept in the sealed tubes, so the amount of each sample did not change. The samples were first annealed at 350 °C for 24 h (blue curves) and then annealed at 400 °C for 48 h (red curves), followed by a final anneal at 450 °C for 80 h (green curves).

https://doi.org/10.1021/acs.inorgchem.2c03703
Inorg. Chem. 2023, 62, 6882−6892

diffusion is ~1 × 10^{18}/cm^3, about a factor of 3 times less than that before diffusion.

By annealing the diffused samples, we can show that the Na is actually still present in the material (Figure 6). A control sample that was not exposed to Li and a Li-diffused sample were annealed in their vacuum-sealed EPR tubes. Each sample was annealed three times, with the temperature and annealing time increasing for each anneal (conditions are given in the caption of Figure 6). EPR spectra were acquired after each anneal. Figure 6a shows EPR spectra of the undiffused sample after each anneal. There is essentially no change after the first and second anneal, as shown in the blue and red curves of Figure 6a. If we heat the sample for a very long time (80 h) at a higher temperature (450 °C) as in the third anneal, the clustered Na feature decreases (Figure S9), but the isolated Na lines are still present with almost the same spin density. For the Li-diffused sample, however, the Na-related EPR features (HF lines and the center peak) returned after annealing, as shown in Figure 6b. We can see, for example, that after the first anneal both the HF lines and the clustered Na feature have nearly returned to their pre-diffusion intensities.

On the basis of the absence of Li-related EPR features and the ability of Li to obscure Na-related features, we speculate that the Li atoms can multiply occupy a cage, forming Li_2 and Li−Na singlet dimers or pairs in a cage that are EPR-silent. We suspect that Li atoms move as ionized atoms during the diffusion and then pair up as the samples cool. These pairs could be thought of as loosely bound molecules with binding energies renormalized by the dielectric environment. The pairs could also form between atoms in adjacent cages. However, undiffused samples exhibit EPR lines from Na−Na dimers in adjacent cages, as mentioned above in Figure 6a. This suggests that, at least for Na, the atoms in adjacent cages do not pair, or if they do interact, the singlet−triplet splitting is too small to avoid populating the triplet states at our measurement temperatures. This observation, along with the small size of Li relative to Na, leads us to suspect that Li atoms tend to pair with other Li or Na atoms in the same cage, while double occupancy of Na atoms in the same cage is much less likely. In fact, electrochemical Li insertion suggested that, at high Li concentration, it is energetically favorable for multiple Li atoms to reside in one single cage.[36] This is also consistent with a previous EPR study of Li and Na ions in zeolites where Na exhibits HF lines, but Li was unobserved in EPR, and this was attributed to pairing.[55] Sato et el. also suggested that Li_2 molecules form in amorphous C electrodes based on the ^{7}Li NMR results.[57] In considering the electrochemical storage of Li in the Si clathrate lattice, this pairing must be taken into account. At the same time, being able to store Li as molecules rather than individual atoms may have advantages in terms of the amount of Li that can be inserted into the Si clathrate lattice.

The recovery of the Na lines when the Li-diffused samples are annealed raises the question of what happens to Li during the anneal. The simplest explanation is that Li leaves the sample. Some out diffusion is likely, but we do not believe that it provides a complete explanation. After annealing, a strong line associated with the presence of free carriers ($g \sim 2.003$) appears and grows in Li-diffused samples (see the red and green curves in Figure 6b and the room temperature spectra in Figure 7). The same growth does not occur in undiffused, Na-doped samples at low temperatures, as shown in Figure 6a. Therefore, we conclude that some Li is still present in the sample and contributing carriers even though a direct signature of the Li atom itself is not observed. A potential explanation involves a strong driving force for Li atoms to continue to pair and cluster, forming locally conducting regions with high free carrier density that show up in the EPR spectrum.

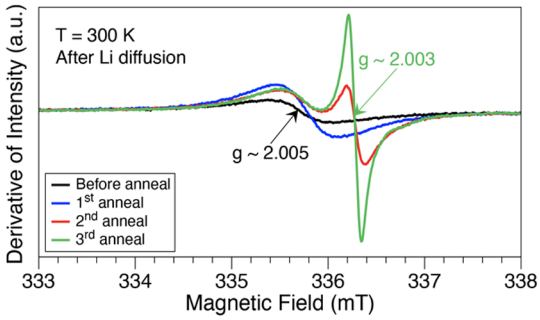

Figure 7. Room temperature EPR spectra of the Li-diffused clathrate film (375 °C for 3.5 h in the sealed ampoule) before and after a series of anneals in the sealed EPR tube. The annealing conditions are described in the caption of Figure 6. All of the spectra were taken at 300 K and averaged over ten scans, with 10^4 gain and 20 dB attenuation.

Another interesting observation from Figure 6a is that the intensity of the disordered Si line near $g \sim 2.005$ decreases as we anneal the undiffused, control sample. This is also observed in room temperature EPR spectra (Figure S10). It could be caused by the formation of Si−Na bonds, with resulting passivation of the dangling bond states or by a shift of the Fermi level, which changes the occupancy of the dangling bond states.[58] We note that after the third anneal of the Na-doped sample, the total spin density is estimated to be 1 × 10^{18}/cm^3, about $x \sim 0.003$ in Na_xSi_{136}, in which nearly 30% of the Na atoms are isolated. This is one of the lowest dopant levels ever observed in Si clathrates. In the Li-doped sample shown in Figure 6b, the relatively strong dangling bond observed after Li diffusion probably arises from the disordered surface material. Changes in its intensity could be caused by either Li breaking Si bonds or Li bonding to the dangling bonds as a form of passivation.

Although the Li diffusion process is not fully understood, a proposed working model for Li diffusion and pairing is given in Figure 8. Before diffusion, isolated Na atoms sitting in a single cage lead to four Na HF lines. During diffusion, Li atoms enter the cages and pair with the Na or form Li−Li dimers, leading to multiple occupancy and spin singlet states that are EPR-silent. This suppresses the Na-related features without creating new Li-related lines. During the post annealing under vacuum, Li continues to move, leaving Na occupied cages, forming clusters of Li atoms, and eventually leading to local conducting regions in the lattice. A fraction of the guests also leave the structure. At this point, the Na-related features in the EPR spectrum have returned. A key conclusion is that Li guests are not simple analogues of Na guests. Li insertion involves more pairing and clustering, which makes it a more complex yet interesting process.

4. CONCLUSION

This work explores thermal diffusion of Li into the guest sites of a nearly empty Si clathrate framework to synthesize Li_xSi_{136}. Starting with an extremely low-Na-content Na_xSi_{136} film, Li diffusion experiments were performed at a range of temperatures. Using TOF-SIMS, we demonstrate Li diffusion profiles

https://doi.org/10.1021/acs.inorgchem.2c03703
Inorg. Chem. 2023, 62, 6882−6892

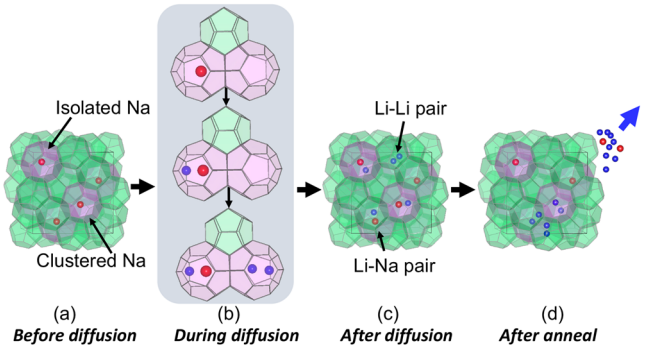

Figure 8. Proposed working model of Li diffusion and pairing. (a) Unit cell of type II Si clathrate before diffusion. Each Na sits in a large cage. For illustrative purposes the figure shows a higher Na concentration than what is actually present. (b) Li pairing during the diffusion. The large and small cages are shaded in pink and green, respectively. The red and blue spheres represent Na and Li atoms, respectively. (c) Unit cell of type II Si clathrate after Li diffusion with the formation of Li_2 and Li−Na pairs. (d) Unit cell of type II Si clathrate after all anneals. The red and blue spheres at the outside edge represent the expelled Na and Li atoms from the clathrate structure.

within the samples that lead to the estimated Li diffusion constants in Si clathrate films. Using XRD, Raman spectroscopy, and EPR, we find evidence of increased doping and the effects of Li insertion on the Si clathrate structure. Our results suggest that Li can be incorporated into the Si clathrate crystal structure using thermal diffusion.

We also found that after diffusion Li ions are present through the thickness of the films. The amount of Li diffused in increases with the temperature and diffusion time, as expected. Effective diffusion constants of Li into the Si clathrate film were estimated based on TOF-SIMS ion profiles.

In the presence of Li, the stability of Si clathrate structure is reduced with the caged structure converting to polycrystalline or disordered Si phases for anneals above 375 °C (or at slightly lower temperatures with higher Li concentration). Li atoms inserted can donate electrons to the Si antibonding state and affect the Si−Si bonds, which was supported by a reduction of the Raman vibrational frequencies. A softening of the Raman modes becomes a convenient way to detect the presence of Li.

Using EPR, we found that Li behaves differently from Na guests in the Si clathrate lattice. Instead of one atom per cage at low guest concentration, our results are consistent with Li atoms tending to form pairs with other Li or Na atoms in a single cage. Thermal Li insertion is not a simple diffusion process but a more complex process involving pairing and clustering. EPR results, consistent with the XRD and Raman results, also suggested that diffusion of Li results in a large increase of the free carrier concentration in the Si clathrate structure.

This is the first time that Li-doped Si clathrate was formed in an alternative approach to the electrochemical method. This systematic study of Li in Si clathrates, coming from a higher-temperature thermodynamically rather than electrochemically driven process, provides new insights into the structural and electronic changes in the clathrate as Li enters the crystal lattice. The results of this work are relevant to the potential use of Si clathrate as an anode material in Li-ion batteries. The procedures and techniques presented also demonstrate a new method for filling the Si clathrate cages, potentially enabling studies of a broad range of other guests in Si clathrates.

■ ASSOCIATED CONTENT

Supporting Information

The Supporting Information is available free of charge at https://pubs.acs.org/doi/10.1021/acs.inorgchem.2c03703.

Additional characterization results, data analysis methods, EASYSPIN simulation, and schematics showing the experimental details (PDF)

■ AUTHOR INFORMATION

Corresponding Author

Carolyn A. Koh − *Department of Chemical and Biological Engineering, Colorado School of Mines, Golden, Colorado 80401, United States;* orcid.org/0000-0003-3452-4032; Email: ckoh@mines.edu

Authors

Yinan Liu − *Department of Chemical and Biological Engineering, Colorado School of Mines, Golden, Colorado 80401, United States;* orcid.org/0000-0002-7128-9089

Joseph P. Briggs − *Department of Chemical and Biological Engineering, Colorado School of Mines, Golden, Colorado 80401, United States*

Ahmad A. A. Majid − *Department of Chemical and Biological Engineering, Colorado School of Mines, Golden, Colorado 80401, United States;* orcid.org/0000-0002-1129-8696

Thomas E. Furtak − *Department of Physics, Colorado School of Mines, Golden, Colorado 80401, United States;* orcid.org/0000-0003-1890-5708

Michael Walker − *Department of Physics, Colorado School of Mines, Golden, Colorado 80401, United States*

Meenakshi Singh − *Department of Physics, Colorado School of Mines, Golden, Colorado 80401, United States*

P. Craig Taylor − *Department of Physics, Colorado School of Mines, Golden, Colorado 80401, United States*

Reuben T. Collins − *Department of Physics, Colorado School of Mines, Golden, Colorado 80401, United States*

Complete contact information is available at: https://pubs.acs.org/10.1021/acs.inorgchem.2c03703

Notes

The authors declare no competing financial interest.

■ ACKNOWLEDGMENTS

This work was supported by the National Science Foundation (Grants 1810463 and 2114569). The materials make use of the TOF-SIMS system at Colorado School of Mines, which was supported by the National Science Foundation under Grant 1726898. The authors thank H. Mikkelson for her help on the Raman measurement and W. K. Schenken for valuable discussions.

■ REFERENCES

(1) Kasper, J. S.; Hagenmuller, P.; Pouchard, M.; Cros, C. Clathrate structure of silicon Na8Si46 and Na x Si136 (x< 11). *Science* **1965**, *150*, 1713−1714.

(2) Cros, C.; Pouchard, M.; Hagenmuller, P. Sur une nouvelle famille de clathrates minéraux isotypes des hydrates de gaz et de liquides. Interprétation des résultats obtenus. *J. Solid State Chem.* **1970**, *2*, 570−581.

https://doi.org/10.1021/acs.inorgchem.2c03703
Inorg. Chem. 2023, 62, 6882−6892

(3) Gryko, J.; McMillan, P. F.; Marzke, R. F.; Ramachandran, G. K.; Patton, D.; Deb, S. K.; Sankey, O. F. Low-density framework form of crystalline silicon with a wide optical band gap. *Phys. Rev. B* **2000**, *62*, R7707.
(4) Yahiro, H.; Yamaji, K.; Shiotani, M.; Yamanaka, S.; Ishikawa, M. An ESR study on the thermal electron excitation of a sodium atom incorporated in a silicon clathrate compound. *Chemical physics letters* **1995**, *246*, 167−170.
(5) Ammar, A.; Cros, C.; Pouchard, M.; Jaussaud, N.; Bassat, J.-M.; Villeneuve, G.; Duttine, M.; Ménétrier, M.; Reny, E. On the clathrate form of elemental silicon, Si136: preparation and characterisation of NaxSi136 (x → 0). *Solid state sciences* **2004**, *6*, 393−400.
(6) Adams, G. B.; O'Keeffe, M.; Demkov, A. A.; Sankey, O. F.; Huang, Y.-M. Wide-band-gap Si in open fourfold-coordinated clathrate structures. *Phys. Rev. B* **1994**, *49*, 8048.
(7) Moriguchi, K.; Munetoh, S.; Shintani, A. First-principles study of Si 34- x Ge x clathrates: Direct wide-gap semiconductors in Si-Ge alloys. *Phys. Rev. B* **2000**, *62*, 7138.
(8) Baranowski, L. L.; Krishna, L.; Martinez, A. D.; Raharjo, T.; Stevanović, V.; Tamboli, A. C.; Toberer, E. S. Synthesis and optical band gaps of alloyed Si−Ge type II clathrates. *Journal of Materials Chemistry C* **2014**, *2*, 3231−3237.
(9) Liu, Y.; Schenken, W. K.; Krishna, L.; Majid, A. A.; Furtak, T. E.; Walker, M.; Koh, C. A.; Taylor, P. C.; Collins, R. T. Synthesis and characterization of type II silicon clathrate films with low Na concentration. *Applied Physics Reviews* **2021**, *8*, 041408.
(10) Kume, T.; Ohashi, F.; Nonomura, S. Group IV clathrates for photovoltaic applications. *Jpn. J. Appl. Phys.* **2017**, *56*, 05DA05.
(11) Martinez, A. D.; Krishna, L.; Baranowski, L. L.; Lusk, M. T.; Toberer, E. S.; Tamboli, A. C. Synthesis of Group IV clathrates for photovoltaics. *IEEE Journal of Photovoltaics* **2013**, *3*, 1305−1310.
(12) Schenken, W. K.; Liu, Y.; Krishna, L.; Majid, A. A.; Koh, C. A.; Taylor, P. C.; Collins, R. T. Electron paramagnetic resonance study of type-II silicon clathrate with low sodium guest concentration. *Phys. Rev. B* **2020**, *101*, 245204.
(13) Guyot, Y.; Champagnon, B.; Reny, E.; Cros, C.; Pouchard, M.; Melinon, P.; Perez, A.; Gregora, I. Raman scattering of silicon clathrates. *Phys. Rev. B* **1998**, *57*, R9475.
(14) Nolas, G.; Kendziora, C.; Gryko, J.; Dong, J.; Myles, C. W.; Poddar, A.; Sankey, O. F. Raman scattering study of stoichiometric Si and Ge type II clathrates. *Journal of applied physics* **2002**, *92*, 7225−7230.
(15) Nolas, G.; Vanderveer, D.; Wilkinson, A.; Cohn, J. Temperature dependent structural and transport properties of the type II clathrates A 8 Na 16 E 136 (A= Cs or Rb and E= Ge or Si). *Journal of applied physics* **2002**, *91*, 8970−8973.
(16) Stefanoski, S.; Beekman, M.; Wong-Ng, W.; Zavalij, P.; Nolas, G. S. Simple approach for selective crystal growth of intermetallic clathrates. *Chem. Mater.* **2011**, *23*, 1491−1495.
(17) Bobev, S.; Sevov, S. C. Clathrates of group 14 with alkali metals: an exploration. *J. Solid State Chem.* **2000**, *153*, 92−105.
(18) Bobev, S.; Sevov, S. C. Synthesis and characterization of stable stoichiometric clathrates of silicon and germanium: Cs8Na16Si136 and Cs8Na16Ge136. *J. Am. Chem. Soc.* **1999**, *121*, 3795−3796.
(19) Kawaji, H.; Horie, H.-o.; Yamanaka, S.; Ishikawa, M. Superconductivity in the silicon clathrate compound (Na, Ba) x S i 46. *Physical review letters* **1995**, *74*, 1427.
(20) Urushiyama, H.; Morito, H.; Yamane, H. Single crystal growth and structure analysis of type-I (Na/Sr)−(Ga/Si) quaternary clathrates. *RSC Adv.* **2019**, *9*, 14586−14591.
(21) Mott, N. Properties of compounds of type NaxSi46 and NaxSi136. *J. Solid State Chem.* **1973**, *6*, 348−351.
(22) Ramachandran, G. K.; Dong, J.; Diefenbacher, J.; Gryko, J.; Marzke, R. F.; Sankey, O. F.; McMillan, P. F. Synthesis and X-ray characterization of silicon clathrates. *J. Solid State Chem.* **1999**, *145*, 716−730.
(23) Roy, S.; Sim, K.; Caplin, A. The insulator-to-metal transition in Si-Na 'clathrate'compounds: A search for superconductivity. *Philosophical Magazine B* **1992**, *65*, 1445−1450.
(24) Ammar, A.; Cros, C.; Pouchard, M.; Jaussaud, N.; Bassat, J.-M.; Villeneuve, G.; Reny, E. Preparation and characterization of the silicon clathrate Na _x Si _{136} (x-> 0). *Journal de Physique IV (Proceedings)* **2005**, *123*, 29−34.
(25) Goebel, T.; Prots, Y.; Haarmann, F. Refinement of the crystal structure of tetrasodium tetrasilicide, Na4Si4. *Zeitschrift für Kristallographie-New Crystal Structures* **2008**, *223*, 187−188.
(26) Beekman, M.; Wei, K.; Nolas, G. S. Clathrates and beyond: Low-density allotropy in crystalline silicon. *Applied Physics Reviews* **2016**, *3*, 040804.
(27) Beekman, M.; Kauzlarich, S. M.; Doherty, L.; Nolas, G. S. Zintl phases as reactive precursors for synthesis of novel silicon and germanium-based materials. *Materials* **2019**, *12*, 1139.
(28) Wen, C. J.; Huggins, R. A. Chemical diffusion in intermediate phases in the lithium-silicon system. *Journal of solid state chemistry* **1981**, *37*, 271−278.
(29) Van der Marel, C.; Vinke, G.; Van der Lugt, W. The phase diagram of the system lithium-silicon. *Solid State Commun.* **1985**, *54*, 917−919.
(30) Beekman, M.; Nolas, G. Inorganic clathrate-II materials of group 14: synthetic routes and physical properties. *J. Mater. Chem.* **2008**, *18*, 842−851.
(31) Langer, T.; Dupke, S.; Trill, H.; Passerini, S.; Eckert, H.; Pöttgen, R.; Winter, M. Electrochemical lithiation of silicon clathrate-II. *J. Electrochem. Soc.* **2012**, *159*, A1318.
(32) Böhme, B.; Reibold, M.; Auffermann, G.; Lichte, H.; Baitinger, M.; Grin, Y. Preparation of anionic clathrate-II K24-xGe136 by filling of Ge (cF136). *Zeitschrift für Kristallographie-Crystalline Materials* **2014**, *229*, 677−686.
(33) Ozanam, F.; Rosso, M. Silicon as anode material for Li-ion batteries. *Materials Science and Engineering: B* **2016**, *213*, 2−11.
(34) Zhao, R.; Bobev, S.; Krishna, L.; Yang, T.; Weller, J. M.; Jing, H.; Chan, C. K. Anodes for Lithium-Ion Batteries Based on Type I Silicon Clathrate Ba8Al16Si30-Role of Processing on Surface Properties and Electrochemical Behavior. *ACS Appl. Mater. Interfaces* **2017**, *9*, 41246−41257.
(35) Warrier, P.; Koh, C. A. Silicon clathrates for lithium ion batteries: A perspective. *Applied Physics Reviews* **2016**, *3*, 040805.
(36) Dopilka, A.; Weller, J. M.; Ovchinnikov, A.; Childs, A.; Bobev, S.; Peng, X.; Chan, C. K. Structural Origin of Reversible Li Insertion in Guest-Free, Type-II Silicon Clathrates. *Advanced Energy and Sustainability Research* **2021**, *2*, 2000114.
(37) Dopilka, A.; Childs, A.; Bobev, S.; Chan, C. K. Electrochemical Lithium Alloying Behavior of Guest-Free Type II Silicon Clathrates. *J. Phys. Chem. C* **2021**, *125*, 19110−19118.
(38) Wagner, N. A.; Raghavan, R.; Zhao, R.; Wei, Q.; Peng, X.; Chan, C. K. Electrochemical cycling of sodium-filled silicon clathrate. *ChemElectroChem.* **2014**, *1*, 347−353.
(39) Dopilka, A.; Zhao, R.; Weller, J. M.; Bobev, S.; Peng, X.; Chan, C. K. Experimental and Computational Study of the Lithiation of Ba8Al y Ge46−y Based Type I Germanium Clathrates. *ACS Appl. Mater. Interfaces* **2018**, *10*, 37981−37993.
(40) Krishna, L.; Baranowski, L. L.; Martinez, A. D.; Koh, C. A.; Taylor, P. C.; Tamboli, A. C.; Toberer, E. S. Efficient route to phase selective synthesis of type II silicon clathrates with low sodium occupancy. *CrystEngComm* **2014**, *16*, 3940−3949.
(41) Yamaga, M.; Kishita, T.; Goto, K.; Sunaba, S.; Kume, T.; Ban, T.; Himeno, R.; Ohashi, F.; Nonomura, S. Electron spin resonance, dynamic Jahn-Teller effect, and electric transport mechanism in Na-doped type II silicon clathrates. *J. Phys. Chem. Solids* **2020**, *140*, 109358.
(42) Reiss, H.; Fuller, C.; Pietruszkiewicz, A. Solubility of lithium in doped and undoped silicon, evidence for compound formation. *J. Chem. Phys.* **1956**, *25*, 650−655.
(43) Wilson, R.; Novak, S. Systematics of secondary-ion-mass spectrometry relative sensitivity factors versus electron affinity and ionization potential for a variety of matrices determined from implanted standards of more than 70 elements. *Journal of applied physics* **1991**, *69*, 466−474.

https://doi.org/10.1021/acs.inorgchem.2c03703
Inorg. Chem. 2023, 62, 6882−6892

(44) Wilson, R.; Stevie, F.; Lux, G.; Kirschbaum, C.; Frank, S.; Pallix, J. Depth profiles, projected ranges, and secondary ion mass spectrometry relative sensitivity factors for more than 50 elements from hydrogen to uranium implanted into metals. *Surf. Coat. Technol.* **1992**, *51*, 358−363.
(45) Baker, J. E.*Practical Materials Characterization*; Springer, 2014; pp 133−187.
(46) Pell, E. Diffusion rate of Li in Si at low temperatures. *Phys. Rev.* **1960**, *119*, 1222.
(47) Vollondat, R.; Roques, S.; Chevalier, C.; Bartringer, J.; Rehspringer, J.-L.; Slaoui, A.; Fix, T. Synthesis and characterization of silicon clathrates of type I Na8Si46 and type II NaxSi136 by thermal decomposition. *J. Alloys Compd.* **2022**, *903*, 163967.
(48) He, J.; Klug, D. D.; Uehara, K.; Preston, K. F.; Ratcliffe, C. I.; Tse, J. S. NMR and X-ray Spectroscopy of Sodium- Silicon Clathrates. *J. Phys. Chem. B* **2001**, *105*, 3475−3485.
(49) Beekman, M. K.Synthesis and Characterization of Type II Silicon and Germanium Clathrates. M.Sc. Thesis, University of South Florida, Tampa, FL, 2006.
(50) Fang, S.; Grigorian, L.; Eklund, P.; Dresselhaus, G.; Dresselhaus, M.; Kawaji, H.; Yamanaka, S. Raman scattering from vibrational modes in Si 46 clathrates. *Phys. Rev. B* **1998**, *57*, 7686.
(51) Beekman, M.; Nolas, G. Synthesis and thermal conductivity of type II silicon clathrates. *Physica B: Condensed Matter* **2006**, *383*, 111−114.
(52) Horie, H.-o.; Kikudome, T.; Teramura, K.; Yamanaka, S. Controlled thermal decomposition of NaSi to derive silicon clathrate compounds. *J. Solid State Chem.* **2009**, *182*, 129−135.
(53) Qu, F.; Li, C.; Wang, Z.; Strunk, H. P.; Maier, J. Metal-induced crystallization of highly corrugated silicon thick films as potential anodes for Li-ion batteries. *ACS Appl. Mater. Interfaces* **2014**, *6*, 8782−8788.
(54) Sim, K. E.Experimental studies of sodium-silicon clathrate compounds. Ph.D. Thesis, Imperial College London, London, U.K., 1983.
(55) Liu, X.; Thomas, J. K. Ionic clusters in γ-irradiated zeolites and their transformation on increasing temperature. *Chemical physics letters* **1992**, *192*, 555−559.
(56) Stoll, S.; Schweiger, A. EasySpin, a comprehensive software package for spectral simulation and analysis in EPR. *Journal of magnetic resonance* **2006**, *178*, 42−55.
(57) Sato, K.; Noguchi, M.; Demachi, A.; Oki, N.; Endo, M. A mechanism of lithium storage in disordered carbons. *Science* **1994**, *264*, 556−558.
(58) Stutzmann, M.; Biegelsen, D.; Street, R. Detailed investigation of doping in hydrogenated amorphous silicon and germanium. *Phys. Rev. B* **1987**, *35*, 5666.

https://doi.org/10.1021/acs.inorgchem.2c03703
Inorg. Chem. 2023, 62, 6882−6892